This paper appears in Mechatronics (Elsevier), 2021.
https://doi.org/10.1016/j.mechatronics.2021.102497

An Admittance-Controlled Wheeled Mobile Manipulator for Mobility Assistance: Human-Robot Interaction Estimation and Redundancy Resolution for Enhanced Force Exertion Ability

Hongjun Xing[a,b], Ali Torabi[b], Liang Ding[a,*], Haibo Gao[a], Zongquan Deng[a], Vivian K. Mushahwar[c], Mahdi Tavakoli[b,*]

[a]*State Key Laboratory of Robotics and System, Harbin Institute of Technology, Harbin 150001, China*
[b]*Department of Electrical and Computer Engineering, University of Alberta, Edmonton T6G 1H9, Alberta, Canada*
[c]*Department of Medicine, Division of Physical Medicine and Rehabilitation, University of Alberta, Edmonton T6G 2E1, Alberta, Canada*

Abstract

In this paper, a novel robotic assistive system (RAS) for mobility assistance of elderly adults is developed based on admittance control with force exertion ability enhancement (FEAE) of a wheeled mobile manipulator (WMM). The RAS can provide supportive force in the vertical direction and be guided by the user with a limited horizontal plane ability. An admittance controller is adopted to realize compliant behaviour between the end-effector and the user, enabling different admittance performances in different directions without requiring the complex system dynamics. The end-effector force needed by the controller is estimated by employing a nonlinear disturbance observer, avoiding the need for pricey force/torque (F/T) sensor. Meanwhile, with consideration of the limited joint torque output, the FEAE approach is implemented in the null-space of the WMM, which can make the system exert more Cartesian force in a given direction with consideration of Cartesian stiffness requirement using the same

*Corresponding authors
Email addresses: xinghj@hit.edu.cn (Hongjun Xing), ali.torabi@ualberta.ca (Ali Torabi), liangding@hit.edu.cn (Liang Ding), gaohaibo@hit.edu.cn (Haibo Gao), dengzq@hit.edu.cn (Zongquan Deng), vivian.mushahwar@ualberta.ca (Vivian K. Mushahwar), mahdi.tavakoli@ualberta.ca (Mahdi Tavakoli)

joint torque limitation through kinematic reconfiguration. Thus, it improves the capability of the system in realizing the desired admittance requirement. The advantages and effectiveness of the proposed approach are experimentally demonstrated with a 4-wheel omnidirectional mobile manipulator.
Keywords: Robotic assistive system, wheeled mobile manipulator, admittance control, human-robot interaction estimation, force exertion ability enhancement.

---

1. Introduction

Seniors and adults with chronic conditions and special needs who have motor capabilities to walk by using an augmentative device are encouraged and recommended to use this ability rather than use a wheelchair to perform their daily living activities [1]. Using a wheelchair causes further muscle weakness, joint stiffness, physiological dysfunctions, and spinal cord deformities. Active rehabilitation and preventing degenerative effects of immobilization depend on how the individuals are urged and supported to walk. These are especially important for older adults as walking prevents functional decline associated with ageing [2]. Furthermore, being active can play a significant role in dealing with the physical health and mental well-being of those in quarantine and isolation during the COVID-19 pandemic [3].

Two of the commonly used augmentative devices that assist people with walking and balance are canes and walkers. These devices enhance the users' stability, support the users' weight, and help them walk. However, traditional walkers and canes suffer from several drawbacks such as requiring sufficient force output to move the device, lack of adaptability with the human motion, collision of the device with the surrounding environment, and short of stability assurance [4, 5].

Here, we propose to employ a wheeled mobile manipulator (WMM), a robotic manipulator mounted on a wheeled mobile, as a robotic assistive system (RAS) to address a portion of the above issues, i.e., the force output enhancement and

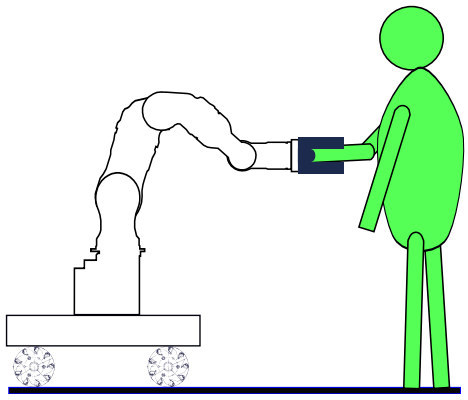

Figure 1: Wheeled mobile manipulator as a robotic assistive system.

the adaptability of the WMM with the human motion. The remained problems will be the focus of our future research. Due to the high mobility and desirable operation capability, WMMs have been widely employed in many applications, including rehabilitation, disaster rescue, and home/service applications [4, 6, 7]. The proposed RAS is designed such that it can be held by one user similar to a cane (see Fig. 1). This can significantly help increase the level of independence and quality of life of seniors and adults with chronic conditions and individual needs. The proposed novel and intelligent system will enable a person with a disability to live independently and carry out everyday activities and tasks. It will also allow caregivers to ensure that the person they are caring for can maintain their independence.

A RAS should achieve different compliant behaviours in different Cartesian directions due to the users' requirements. In terms of the robotic walking assistance system, Itadera *et al.* [4] proposed a WMM to provide walking assistance for elderly adults through predictive optimization of gait assistive force. However, the compliance was only realized in a single direction, and the implementation needed a wrist force/torque (F/T) sensor. Zhu *et al.* [8] presented an admittance control-based approach for walking support and power assistance with a wheelchair typed robot without assigning the desired stiffness of the sys-

tem. Spenko *et al.* [9] proposed a mobile robot based robotic system to provide support and guidance for the elderly with the requirement of a wrist F/T sensor. Frizera *et al.* [10] designed a "Smart Walker" to provide support for cognitive disabilities and people who cannot utilize conventional walkers. By employing an admittance controller, the walker could generate haptic signals to help track a predetermined path; however, the drawbacks of the traditional mobile platform typed walkers still existed in this robotic system.

Compliant control is a desirable approach to realize compliant behaviour between the robot and the environment. Two fundamental methods are proposed based on hybrid position/force control [11] and impedance control [12]. To achieve impedance behaviour in all Cartesian directions and avoid the requirement of complex system dynamics, admittance control [13, 14] is adopted in this paper. And it should be noted that impedance control and admittance control are two ways of implementing impedance control, depending on the causality of the controller [13]. Admittance control has found many applications including in upper limb rehabilitation [15], walk-assist [4], and robotic teleoperation system [16]. One issue about implementing admittance control is the end-effector force requirement because it serves as the input for the controller to derive the desirable compliant behaviour.

Besides mounting a pricey wrist F/T sensor, many other estimation methods have been presented based on the robot's available sensing. Disturbance observer (DOB) is one of the methods used in the external force estimation of robots [17, 18]. A general review of DOB theory could be found in [19]. One technique is the time delay estimation method that could be used to estimate the nonlinear dynamics of the manipulator [20]. Another method for force estimation is based on generalized momentum, which avoids joint acceleration measurement [21, 22]. Haddadin *et al.* [23] reviewed and extended this method for real-time collision detection, isolation, and identification, yet they have failed to provide the convergence verification of this approach. If the system is in quasi-static mode or moves very slowly, the external force estimation can be achieved via simple gravity and joint friction compensation [24].

Due to the limited and inequable joint torque output of the manipulator, the manipulator's configuration should be adjusted to derive the end-effector's optimal impedance behaviour. The null-space controller can be adopted to execute multiple tasks, thanks to the redundancy of the WMM system [25]. Many studies have been conducted about redundancy applications, such as force feedback improvement, manipulability maximization, and singularity avoidance [26, 27, 28]. The robotic system's force exertion ability in a given direction should be enhanced to achieve better impedance behaviour, indicating the robotic system can sustain a more significant end-effector force within the joint actuation saturation. The force manipulability ellipsoid, first proposed by Yoshikawa [28], is a useful tool for visualizing the force transmission characteristics of a robot at a given configuration [29]. Later, the applications of this measure have been extended to mobile manipulators [30]. However, this measure always tries to evaluate the system force capability in all Cartesian directions, which is not needed in our application. To solve this problem, the concept of task compatibility, which optimizes the velocity or force requirements in a given direction, was presented by Chiu [31], and Ajoudani *et al.* [32] improved this concept by introducing a weighting matrix to scale the joint torques because of the joint torque differences.

A fundamental problem with much of the literature regarding the walking assistance system is that only a mobile platform type robot is employed [5, 9], which dramatically limits the system's functionality. Even with a WMM, the redundancy of the system has not been considered [4]. Another drawback impeding the high-quality of the RAS system is the restricted joint torque output of the manipulator. This problem can be solved using the null-space control of the robotic system; however, to the best of our knowledge, no research about this topic has been conducted.

In this paper, a novel method to achieve a RAS via admittance control with consideration of force exertion ability enhancement (FEAE) is proposed. It is noteworthy that the required force for an applicable robotic walker is approximately in the range of 60 N [33] to 150 N [34]. The main contributions of

the paper are as follows: (1) From an application perspective, implementing a WMM without a F/T sensor as a RAS is novel compared to the past research that typically employs a mobile robot or a wheelchair as assistive technology; (2) from a theoretical point of view, the proposed combination of admittance control in the Cartesian space and null-space control is novel and of great significance in improving the robotic system's performance in terms of (a) showing a compliant behaviour in the horizontal plane such that the WMM does not resist user's motions in the left-right or the back-forth directions and (b) showing a stiff behaviour in the vertical direction such that the WMM provides support to the user; and (3) a null-space configuration optimization approach is proposed to enhance the end-effector force exertion capability in the vertical direction with consideration of stiffness requirements.

The remainder of this paper is organized as follows. In Section 2, the kinematic model and control for WMMs are provided. In Section 3, an admittance control for WMMs with force exertion ability enhancement is presented. Experiments that demonstrate the validity and performance of the proposed method are presented in Section 4. Section 5 concludes the manuscript.

2. Kinematics for Wheeled Mobile Manipulators

An intelligent RAS should have the ability to sense the force exerted by the user and change its configuration to follow the user's motion. Thus, the kinematic modelling and control method is needed for the WMM. In this section, a unified kinematic model and control approach for a WMM is derived, which avoids the complex system dynamics and plays an essential role in the Cartesian space controller design in the following section. First, the kinematic model for the WMM is obtained. Next, a kinematic controller is presented, including the Cartesian space controller and the null-space controller, which will be utilized to realize the desirable admittance behaviour and augment the end-effector force exertion ability, respectively.

A WMM consists of a mobile base and a multi-DOF manipulator, as shown

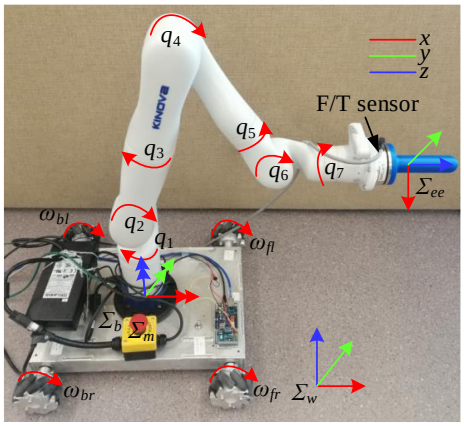

Figure 2: Kinematic model representation of the mobile manipulator.

in Fig. 2, in which Σ_w, Σ_b, Σ_m, and Σ_{ee} represent the world reference frame, mobile base frame, manipulator reference frame, and end-effector frame, respectively. It is worth mentioning that in each frame, the red, green, and blue pointing arrows denote its corresponding x, y, and z, respectively. Let us define $q = [q_b^{\mathrm{T}}, q_m^{\mathrm{T}}]^{\mathrm{T}} \in \mathbb{R}^n$ as the configuration vector of the WMM, where $q_b \in \mathbb{R}^{n_b}$ and $q_m \in \mathbb{R}^{n_m}$ are the generalized coordinates of the base and the manipulator, respectively, in which, $n = n_b + n_m$, where n_m and n_b denote the dimensions of the generalized coordinates for the manipulator and the mobile base, respectively. Then, the pose of the end-effector $x \in \mathbb{R}^r$ can be expressed as $x = f(q)$, where $f(q)$ denotes the forward kinematics for the WMM system and r represents the dimension of the end-effector's motion.

We assume that a pure rolling contact exists between the mobile base's wheels and the ground (i.e., no slippage). The model for slippery wheels can be found in other literature from our group [35]. With this assumption, the mobile base kinematic model can be derived as $\dot{q}_b = P(q_b)u_b$, where $u_b \in \mathbb{R}^b$ is the velocity vector of the wheels with b denoting its dimension, and $P(q_b) \in \mathbb{R}^{n_b \times b}$ is the constraint matrix of the base (holonomic or nonholonomic). The generalized velocity vector for the manipulator can be expressed via the joint velocity vector as $\dot{q}_m = u_m$, where $u_m \in \mathbb{R}^m$ is the velocity vector of the manipulator joints with

m representing the dimension of the manipulator velocity inputs ($m = n_m$).

Thus, by defining the velocity input vector for the WMM as $u = [u_b^{\mathrm{T}}, u_m^{\mathrm{T}}]^{\mathrm{T}} \in \mathbb{R}^{b+m}$, the forward kinematics at velocity level for the entire WMM can be expressed as

$$\begin{aligned} \dot{x} = J(q)\dot{q} &= [J_b(q)\ J_m(q)] \begin{bmatrix} \dot{q}_b \\ \dot{q}_m \end{bmatrix} \\ &= [J_b(q)P(q_b)\ J_m(q)] \begin{bmatrix} u_b \\ u_m \end{bmatrix} = J_u(q)u, \end{aligned} \tag{1}$$

in which $J_b \in \mathbb{R}^{r \times n_b}$ is the Jacobian of the mobile base, $J_m \in \mathbb{R}^{r \times m}$ is the Jacobian of the manipulator, $J(q) \in \mathbb{R}^{r \times n}$ is the Jacobian of the generalized WMM (i.e., no constraints for the mobile base are considered), and $J_u(q) \in \mathbb{R}^{r \times (b+m)}$ is the Jacobian of the WMM. It is worth mentioning that for a holonomic mobile base, the utilization of $J(q)$ and $J_u(q)$ have the same efficiency.

As shown in (1), for a WMM, the Jacobian matrix $J(q)$ has more columns than rows, indicating that the WMM system is kinetically redundant. Therefore, for a given end-effector trajectory tracking task $\dot{x}$, infinite joint velocity solutions $\dot{q}$ can be obtained. To determine the optimal joint trajectory, the redundancy resolution approaches for redundant manipulators can be extended to the kinematic control of the WMM [21].

With the reference end-effector velocity vector defined as $\dot{x}_r$, the redundancy resolution for the WMM expressed in (1) can be derived as[1]

$$\dot{q} = J^{\dagger}\dot{x}_r + (I - J^{\dagger}J)\dot{q}_N, \tag{2}$$

where $J^{\dagger}$ denotes the pseudoinverse of Jacobian J, $I - J^{\dagger}J$ denotes the orthogonal projection operator into $\mathcal{N}(J)$, and $\dot{q}_N$ represents the designed joint velocity vector for the secondary task.

Joint position constraint avoidance cannot be realized via the pseudoinverse method discussed above when joint position limit is reached. Two other control

[1]For brevity, the dependence of the variables upon the joint variables are omitted.

methods can be adopted for this case. One is Hierarchical Quadratic Programming (HQP) [36], which is often implemented for robots to inverse a direct function when multiple and incompatible objectives are involved. The other one is the addition of an optimization objective for joint position limit avoidance [27]. With the implementation of a WMM as a RAS, the end-effector motion in the vertical direction is small to support the user. The horizontal plane's movement is mostly distributed to the mobile base, which has an unlimited joint motion range. Thus, in our work, the manipulator does not reach its joint position limit.

Furthermore, to track a desired trajectory provided by both the desired end-effector position $x_d(t)$ and the desired end-effector velocity $\dot{x}_d(t)$, a closed-loop controller [37] can be employed to restate $\dot{x}_r$ in (2) as

$$\dot{x}_r(t) = \dot{x}_d(t) + K_x\big(x_d(t) - x(t)\big), \tag{3}$$

where K_x is a constant gain scalar.

3. Admittance Control for WMMs with Force Exertion Ability Enhancement

This section's primary purpose is to design an appropriate controller to realize the desired user-defined compliant behaviour for the RAS. We are starting with the presentation of the admittance controller, which avoids the complicated dynamics modelling of the WMM compared with the impedance controller [12]. With this basic control framework, we design an end-effector force estimator via NDOB. An FEAE approach is then presented to augment the Cartesian force exertion capability in a given direction using the null-space controller to cope with the limited joint torque output.

3.1. Admittance Control for WMMs

Admittance control can help adjust the position (orientation) of the end-effector according to the external force (torque); thus, it can assist walking for

the elderly by generating compliant behaviours between the user and the robotic system. In this paper, only position compliance is considered according to the external force, with the end-effector's orientation always kept unchanged. The transfer function of an admittance controller that specifies the control velocity vector can be expressed as

$$\frac{\dot{x}(s)}{f(s)} = R(s) = \frac{s}{M_d s^2 + B_d s + K_d}, \tag{4}$$

where $f \in \mathbb{R}^3$ denotes the external force vector. $M_d \in \mathbb{R}^{3\times3}$, $B_d \in \mathbb{R}^{3\times3}$, and $K_d \in \mathbb{R}^{3\times3}$ are diagonal matrices representing the desired Cartesian inertial, damping, and stiffness, respectively. Then, by exerting an end-effector force f_e to the robotic system, the admittance controller will generate a reference Cartesian velocity vector $\dot{x}_e$ to adjust the end-effector position.

To avoid the user discomfort with small differences in end-effector position and the user's desired position, the admittance behaviour (4) is directly applied to the system as in [38]. Thus, the desired end-effector velocity can be defined as

$$\dot{x}_d(t) = \dot{x}_{d,User}(t) + \dot{x}_e(t), \tag{5}$$

where $\dot{x}_{d,User}(t)$ is the velocity vector assigned by the user, and $\dot{x}_e(t)$ can be obtained by acquiring the end-effector force, which will be estimated using a nonlinear disturbance observer in Section 3.2.

3.2. End-effector Force Estimation via Nonlinear Disturbance Observer

When no F/T sensor is available at the end-effector, an alternative method for obtaining the external force is provided by designing a suitable NDOB, which considers the external force as the disturbance. The NDOB adopted in this paper is inspired by the work reported in [18, 39]. Reference [18] removed the existing restrictions of [39] on the number of DOFs, joint types, or manipulator configuration. Compare with the work in [18], the joint torque is also modeled in this paper to further improve the force estimation accuracy.

Assumption 1: The dynamics of the mobile base are separated from the entire WMM system's dynamics. Thus, the end-effector force estimation will

be conducted only considering the manipulator[2].

The complete dynamic model of an m-DOF manipulator is expressed as [40]

$$M(q_m)\ddot{q}_m + N(q_m, \dot{q}_m) = \tau_m + \tau_e \tag{6}$$

with

$$N(q_m, \dot{q}_m) = C(q_m, \dot{q}_m)\dot{q}_m + G(q_m) + F(q_m, \dot{q}_m), \tag{7}$$

where $M(q_m) \in \mathbb{R}^{m\times m}$, $C(q_m, \dot{q}_m) \in \mathbb{R}^{m\times m}$, and $G(q_m) \in \mathbb{R}^m$ denote the inertia matrix, Coriolis and centrifugal terms, and gravity term of the manipulator, respectively. $F(q_m, \dot{q}_m) \in \mathbb{R}^m$ denotes the friction torque vector of the joints, $\tau_m \in \mathbb{R}^m$ denotes the joint control torque vector, and $\tau_e \in \mathbb{R}^m$ is the resultant joint torque vector exerted by the external force.

The friction model to estimate the joint friction torque $F(q_m, \dot{q}_m)$ adopted in this paper is expressed as [41]

$$F(q_m, \dot{q}_m) = \left[f_c + (f_s - f_c)e^{-|\dot{q}_m/v_s|^2}\right]\mathrm{sgn}(\dot{q}_m) + f_v\dot{q}_m, \tag{8}$$

where f_c, f_s and f_v represent the Coulomb, static and viscous friction coefficients, respectively, and the parameter v_s denotes the Stribeck velocity.

Now, define the estimates of the actual $M(q_m)$ and $N(q_m, \dot{q}_m)$ as $\hat{M}(q_m)$ and $\hat{N}(q_m, \dot{q}_m)$, and $\tilde{M}$ and $\tilde{N}$ denote the corresponding additive uncertainties exist in (6), which yield

$$\begin{aligned} M(q_m) &= \hat{M}(q_m) + \tilde{M}, \\ N(q_m, \dot{q}_m) &= \hat{N}(q_m, \dot{q}_m) + \tilde{N}. \end{aligned} \tag{9}$$

The lumped disturbance vector $\tau_d \in \mathbb{R}^m$ is defined as

$$\tau_d = \tau_e - \tilde{M}\ddot{q}_m - \tilde{N}, \tag{10}$$

[2]This assumption is feasible since, for a collaborative WMM moving with low velocity, most of the joint torques are caused by gravity and joint friction. In contrast, the influence of dynamics is tiny.

thus, with a desirable estimation of $M(q_m)$ and $N(q_m, \dot{q}_m)$, the resultant joint torque vector τ_e by external force is almost equal to τ_d according to (10). Combining (6) and (10), it derives

$$\hat{M}(q_m)\ddot{q}_m + \hat{N}(q_m, \dot{q}_m) = \tau_m + \tau_d. \tag{11}$$

It is worth mentioning that $\hat{M}(q_m)$ is a positive-definite and symmetric matrix. Then, a nonlinear disturbance observer is proposed as

$$\dot{\hat{\tau}}_d = -L\hat{\tau}_d + L[\hat{M}(q_m)\ddot{q}_m + \hat{N}(q_m, \dot{q}_m) - \tau_m], \tag{12}$$

where $L \in \mathbb{R}^{m\times m}$ is a constant observer gain matrix. Inspired by the method proposed in [18], an auxiliary variable $z \in \mathbb{R}^m$ is defined to avoid joint acceleration measurement in (12). The modified disturbance observer is built as

$$z = \hat{\tau}_d - p(q_m, \dot{q}_m), \tag{13}$$

where the vector $p(q_m, \dot{q}_m) \in \mathbb{R}^m$ is determined from a modified observer gain matrix $L(q_m, \dot{q}_m) \in \mathbb{R}^{m\times m}$

$$\dot{p}(q_m, \dot{q}_m) = L(q_m, \dot{q}_m)\hat{M}(q_m)\ddot{q}_m. \tag{14}$$

Combining (11), (12), (14), and taking the time derivative of (13) yields

$$\begin{aligned}\dot{z} =& \dot{\hat{\tau}}_d - \dot{p}(q_m, \dot{q}_m) = \dot{\hat{\tau}}_d - L(q_m, \dot{q}_m)\hat{M}(q_m)\ddot{q}_m \\ =& -L(q_m, \dot{q}_m)z + \\ & L(q_m, \dot{q}_m)[\hat{N}(q_m, \dot{q}_m) - \tau_m - p(q_m, \dot{q}_m)].\end{aligned} \tag{15}$$

Thus, the modified disturbance observer, which eliminates the joint accelerometer requirement, is established with the following form

$$\begin{aligned}\dot{z} =& -L(q_m, \dot{q}_m)z + \\ & L(q_m, \dot{q}_m)[\hat{N}(q_m, \dot{q}_m) - \tau_m - p(q_m, \dot{q}_m)], \\ \hat{\tau}_d =& z + p(q_m, \dot{q}_m), \\ \dot{p}(q_m, \dot{q}_m) =& L(q_m, \dot{q}_m)\hat{M}(q_m)\ddot{q}_m.\end{aligned} \tag{16}$$

Next, the error dynamics of the system can be obtained as

$$\dot{\tilde{\tau}}_d = \dot{\tau}_d - \dot{\hat{\tau}}_d = \dot{\tau}_d - L(q_m, \dot{q}_m)\tilde{\tau}_d. \tag{17}$$

The vector $p(q_m, \dot{q}_m)$ and the matrix $L(q_m, \dot{q}_m)$ in (16) are undetermined, and now an approach for their design is provided. In line with [18], the modified observer gain matrix is presented as

$$L(q_m) = X^{-1}\hat{M}^{-1}(q_m), \tag{18}$$

where $X \in \mathbb{R}^{m\times m}$ is a constant invertible matrix, and $\hat{M}(q_m)$ is an invertible matrix as well. Combining (14) and (18) yields

$$p(\dot{q}_m) = X^{-1}\dot{q}_m. \tag{19}$$

The disturbance tracking error $\tilde{\tau}_d$ will converge asymptotically to zero if the invertible matrix X is chosen with the following condition

$$X + X^{\mathrm{T}} \geqslant X^{\mathrm{T}}\dot{\hat{M}}(q_m)X, \tag{20}$$

and the rate of change of the lumped disturbance acting on the manipulator ought to be negligible compared with the estimation error dynamics (17), which is not an overly restrictive condition [39]. The proof of this conclusion can be found in [18].

According to (10), (16), (18), (19), and with the assumption that a desirable estimation of $M(q_m)$ and $N(q_m, \dot{q}_m)$ can be derived, the end-effector force (torque) vector $F_e \in \mathbb{R}^r$ can be estimated as

$$F_e = {J_m^{\mathrm{T}}}^{\dagger}\hat{\tau}_d, \tag{21}$$

in which, we denote $f_e \in \mathbb{R}^3$ as the force component of F_e.

3.3. Force Exertion Ability Enhancement with Null-space Control

With the admittance controller employed in the Cartesian space of the WMM, the desired admittance behaviour should be achieved for assistance in walking. However, due to the manipulator's limited joint torque output, some

Cartesian motion requirement may not be satisfied. Hence, the redundant system's null-space control can be used to enhance the force exertion ability of the end-effector. It should be noted that the torque output of the mobile base is assumed to be unlimited and not considered in this section because the base cannot help to adjust the admittance behaviour for the user in the vertical direction.

Consider the manipulator is stable with joint position q_m and $\tau_m = J_m^{\mathrm{T}}(q_m) f_e + \tau_g(q_m)$, where τ_m is the control torque vector of the manipulator and $\tau_g(q_m)$ denotes the gravity vector exerted by the manipulator. The joint friction is neglected as this is a static equilibrium analysis.

To account for the torque limit difference of the manipulator joints, the joint torque output can be scaled as

$$\tau_{mw} = W_\tau \tau_m, \tag{22}$$

where $W_\tau = \mathrm{diag}[\frac{1}{\tau_{m\,\mathrm{lim}_1}} \ \frac{1}{\tau_{m\,\mathrm{lim}_2}} \ \cdots \ \frac{1}{\tau_{m\,\mathrm{lim}_m}}]$ is a scaling matrix to normalize the joint torques, and $\tau_{m\,\mathrm{lim}_i}$ represents the torque limit of the i^{th} joint. In line with the definition of the force manipulability ellipsoid in [31], i.e., $\|\tau_{mw}\|_2 \leqslant 1$, the joint torque constraint can be rewritten as [32]

$$[W_\tau (J_m^{\mathrm{T}} f_e + \tau_g)]^{\mathrm{T}} [W_\tau (J_m^{\mathrm{T}} f_e + \tau_g)] \leqslant 1, \tag{23}$$

where τ_g can be expressed as $\tau_g = J_m^{\mathrm{T}} G_q$. (23) can be further expressed as

$$(f_e + G_q)^{\mathrm{T}} J_m W_\tau W_\tau J_m^{\mathrm{T}} (f_e + G_q) \leqslant 1. \tag{24}$$

Then, with the assumption that the stiffness of the end-effector is $K_c \in \mathbb{R}^{3\times3}$, i.e., $f_e = K_c \Delta x$, (24) can be restated as

$$(\Delta x + \Delta x_g)^{\mathrm{T}} K_c J_m W_\tau W_\tau J_m^{\mathrm{T}} K_c (\Delta x + \Delta x_g) \leqslant 1 \tag{25}$$

with

$$\Delta x_g = K_c^{-1} G_q. \tag{26}$$

In order to enhance the end-effector force exertion capability with consideration of stiffness requirements in different Cartesian directions, a scalar optimization

objective can be defined as

$$H_1 = [\delta^{\mathrm{T}}(K_c J_m W_\tau W_\tau J_m^{\mathrm{T}} K_c)\delta]^{-1}, \tag{27}$$

where $\delta \in \mathbb{R}^3$ is a vector of 0 and 1 representing the Cartesian direction of the optimization. It is worth mentioning that K_c only represents a stiffness for the optimization of the end-effector. In this paper, the force exertion capability is not enhanced directly. It is augmented through enlarging the maximum end-effector allowable displacement within the joint actuation saturation. In essence, the permissible end-effector force is enhanced. It is evident that with the joint torque constraint presented in (25) and the optimization objective proposed in (27), the enhanced displacement also contains the one caused by the manipulator gravity, i.e., Δx_g. Therefore, another goal is defined to reduce the effect of gravity, which is expressed as

$$H_2 = \Delta x_g^{\mathrm{T}} \Delta x_g / \alpha, \tag{28}$$

where α is a scalar gain, which makes objectives H_1 and H_2 on the same order of magnitude. Combining (27) and (28), the cost function for the null-space controller can be defined as

$$H = w_1 H_1 - w_2 H_2, \tag{29}$$

where w_1 and w_2 are two constant gains with $w_1 + w_2 = 1$; w_1 ought to be bigger than w_2 since augmentation of force ability is the main task. By calculating the partial derivative of H to q_m, denoting as $\nabla_{q_m} H$, we can obtain the designed joint velocity vector for FEAE as

$$\dot{q}_N = k_N \begin{bmatrix} 0_{n_b \times 1} \\ (\nabla_{q_m} H)^{\mathrm{T}} \end{bmatrix} \tag{30}$$

with k_N being a constant gain. With the optimization of the cost function defined in (29), only the Cartesian displacement introduced by the external force will be enhanced. The block diagram of the entire control system is shown in Fig. 3.

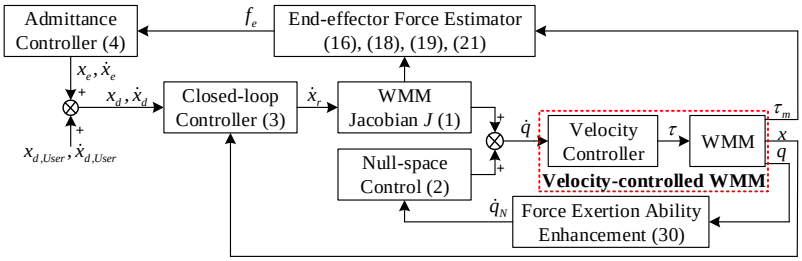

Figure 3: Block diagram of the control system.

4. Experimental Setup and Results

Several experiments are conducted to verify the effectiveness of the proposed method with a WMM for achieving a RAS. The experiments in this section contain two parts: (A) the verification of the FEAE approach to improve the admittance performance and (B) the evaluation of the admittance controller in terms of providing supportive force and guidance.

4.1. Experimental Setup

In this study, an omnidirectional wheeled mobile manipulator (holonomic constraint for the base) is utilized (shown in Fig. 2), which consists of a custom-built four-wheel mobile base, a 7-DOF ultra-lightweight robotic arm Kinova Gen3 (Kinova Robotics, Canada), and an Axia80-ZC22 F/T sensor (ATI Industrial Automation, Apex, NC, USA). The mobile base is equipped with two pairs of Mecanum wheels to realize omnidirectional motion, which shortens robot throughput times and reduces nonproductive time when searching appropriate execution pose for a given task [42]. The F/T sensor is employed to evaluate the accuracy of the force estimation method and not used in the control system.

The generalized coordinate vector for the mobile base (shown in Fig. 4) is defined as $q_b = [x_b, y_b, \theta_b]^{\mathrm{T}} \in \mathbb{R}^3$. Also, the velocity command of the wheels is defined as $u_b = [\omega_{fl}, \omega_{fr}, \omega_{bl}, \omega_{br}]^{\mathrm{T}} \in \mathbb{R}^4$. The velocity transformation matrix $P(q_b) \in \mathbb{R}^{3\times4}$, which transfers the wheel velocities to the generalized base

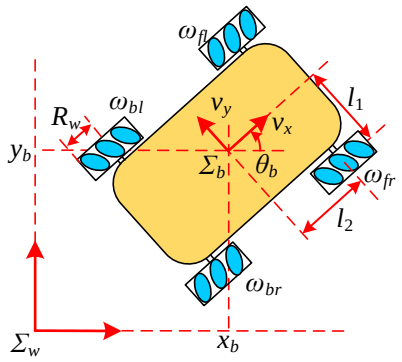

Figure 4: Kinematics of the omnidirectional mobile base.

velocities, can be expressed as

$$P(q_b) = J_I J_B \tag{31}$$

with $J_I = \begin{bmatrix} \cos\theta_b & -\sin\theta_b & 0 \\ \sin\theta_b & \cos\theta_b & 0 \\ 0 & 0 & 1 \end{bmatrix}$, and $J_B = \frac{R_w}{4} \begin{bmatrix} 1 & 1 & 1 & 1 \\ -1 & 1 & 1 & -1 \\ \frac{-1}{l_1+l_2} & \frac{1}{l_1+l_2} & \frac{-1}{l_1+l_2} & \frac{1}{l_1+l_2} \end{bmatrix}$.
The variables θ_b, R_w, l_1, and l_2 are illustrated in Fig. 4.

The Cartesian space dimension for the mobile manipulator is defined to be $r = 6$ considering both the position and orientation of the end-effector. Yet, only the position compliance is treated, and for the orientation, a simple PD controller is employed to maintain it fixed. At the initial point, we assume that the mobile base frame Σ_b is coincident with the world frame Σ_w. The initial joint position of the WMM is considered as $q_0 = [0, 0, 0, 0, \pi/6, 0, \pi/2, 0, -\pi/6, 0]^{\mathrm{T}}$, where the first three values are the generalized coordinates for the mobile base. The initial position for the end-effector can be derived from the system forward kinematics in Σ_w as $x_0 = [0.65, -0.0246, 0.4921]^{\mathrm{T}}$.

4.2. Experiment on Force Exertion Ability Enhancement with Null-space Control

Based on the proposed approach of admittance control with estimated end-effector force, the desired Cartesian impedance behaviour of the end-effector can

be achieved. However, some desirable responses of the admittance controller may not be gained due to the manipulator's limited joint torque output. Thus, in this experiment, the system redundancy is employed to augment the force exertion capability of the end-effector in a given direction through null-space control.

This experiment shows that with the proposed FEAE approach, the WMM will change into a more desirable configuration for mobility assistance, and only the WMM configuration evolution with no user interference is considered. A video is attached to the manuscript to present this experiment. In this paper, the FEAE method is used in the vertical direction because this direction should provide a sizeable supportive force for the users to assist them in walking.

The parameters used during the experiment are listed in Table 1, where K_c does not represent the real Cartesian stiffness for the admittance controller but a stiffness for the configuration optimization procedure, which is obvious that we put our focus on z direction; and the optimization direction vector is defined as $\delta = [0, 0, 1]^{\mathrm{T}} \in \mathbb{R}^3$ to enhance the Cartesian displacement along the z direction of the world frame Σ_w (shown in Fig. 2). If otherwise stated, the reference frame of the direction is the world frame in the subsequent expression. It should be emphasized that the desired Cartesian position for the end-effector is unchanged in this experiment. The reason lies in two aspects. First, no user influence is added in this experiment. Second, we want to show that by employing FEAE, we can use less joint torque output to obtain the same end-effector force exertion capability without affecting its Cartesian position.

The results of the WMM augmenting the force exertion ability in the z direction of Σ_w are as follows. Fig. 5 shows the final configuration of the WMM without and with FEAE. Fig. 5b shows that with the proposed method, the manipulator will go to a more desirable configuration to augment the force exertion capability of the end-effector in z. This is similar to how humans change their configuration to resist disturbance from the vertical direction.

The optimization objective and norm of the weighted joint torque profiles are shown in Fig. 6. Fig. 6a depicts the objective profile defined in (27)-(29) during

Table 1: Control parameters for force exertion ability enhancement experiment.

Parameter	Description	Value
K_c	Stiffness for optimization	$\mathrm{diag}(1, 1, 10)$
K_x	Closed-loop controller gain	10
W_τ	Torque scaling matrix	$\mathrm{diag}(1, 1, 1, 1, 2.5, 2.5, 2.5)$
k_N	Null-space controller gain	5
δ	Optimization direction vector	$[0, 0, 1]^{\mathrm{T}}$
α	Gravity effect gain	10000
w_1	Objective ratio for H_1	0.9
w_2	Objective ratio for H_2	0.1
X	Matrix for force estimation	$100I_{7\times7}$

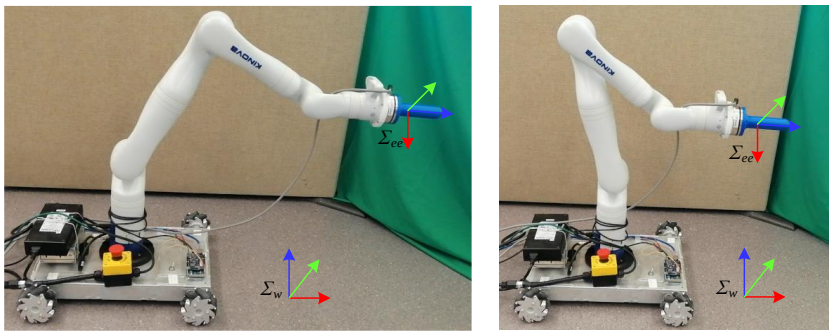

(a) Without FEAE (b) With FEAE

Figure 5: Final configurations of the WMM during the experiment.

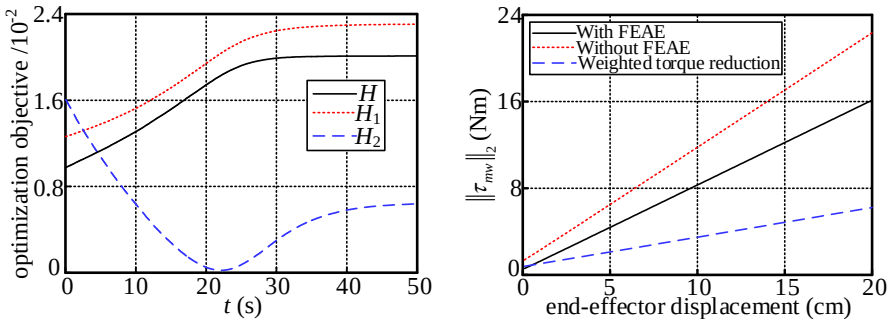

(a) Optimization objective

(b) Norm of weighted torque

Figure 6: Optimization objective and norm of the weighted joint torque during the experiment.

the FEAE experiment. With the proposed method, the cost function H was enhanced from 0.978×10^{-2} to 2.012×10^{-2}, more than twice as before, which means the manipulator could achieve the same Cartesian displacement in z with less joint torque output. It is worth noting that there were two sub-objectives in the cost function, H_1 and H_2, and H_2 had an increasing tendency in the later period of the experiment due to its small weighting value w_2. Fig. 6b shows the norm of the required weighted joint torque when end-effector displacement in z was generated, where the desired stiffness in this direction was set as 1500 N/m. Two manipulator configurations (the initial and final configurations) were compared. When no external displacement was applied, the gravity-related $\|\tau_{mw}\|_2$ was reduced from 1.39 Nm to 0.59 Nm with FEAE, and the increasing speed of the weighted joint torque with z displacement was also declined from 104.8 N to 77.7 N. When the required end-effector displacement increased to 20 cm, the reduction of the weighted joint torque was 6.2 Nm, approximately 27.7% of the original value. Both of these two results illustrate the effectiveness of the proposed method in enhancing the force exertion ability for the end-effector.

4.3. Experiment on Admittance Control with Estimated End-effector Force

In this section, the WMM performance used as a RAS is verified to provide supportive force in the vertical direction by a known payload and be guided in the horizontal direction by a user.

This experiment compares the admittance behaviors with two different final WMM configurations (without FEAE and with FEAE). The process of how the WMM configuration evolved via FEAE is not presented here since it is already shown in the first experiment, and a video is attached to show this experiment.

The user-defined trajectory $x_{d,User}$ is set as the initial end-effector position x_0 to better display the impedance behaviour of the WMM produced by the external force. The control parameters are listed in Table 1 with the desired Cartesian impedance parameters defined as $M_d = \text{diag}(100, 100, 100)\,\text{Ns}^2/\text{m}$, $B_d = \text{diag}(200, 200, 550)\,\text{Ns/m}$, and $K_d = \text{diag}(0, 0, 1500)\,\text{N/m}$. It should be emphasized that the desired stiffness in x and y is defined as zero to ensure that the robotic system can be led by the user smoothly in the horizontal plane. The advantages of the proposed method have been experimentally compared with the traditional admittance control without FEAE ((3), (4), (5), and (2) without employing the null-space controller). Due to the existing end-effector force estimation error, if the estimated external force is less than 3 N in each Cartesian direction, it is assumed to be zero.

The first segment is to prove the accuracy of the end-effector force estimation approach with NDOB, the estimated force (calculated via (16), (18), (19), and (21)) is compared with the measured force obtained by the wrist F/T sensor.

The WMM configuration with FEAE was chosen to compare the estimated and measured forces, where the user exerted the external force in different directions. The experimental results are shown in Fig. 7. Table 2 contains the maximum and RMS values of the estimation errors in each direction. During the experiment, the user first applied the force in z direction, then, in y direction, and finally in x direction.

As shown in Fig. 7 and Table 2, the maximum Cartesian space force estimation errors between the estimated forces and the force measurements in x, y, and z are 3.34 N, 3.02 N, and 4.56 N, respectively. The RMS level of these estimation errors is 1.14 N, 0.91 N, and 1.02 N, respectively, which accounts for about 7.06%, 6.80%, and 4.93% of their corresponding maximum force measurements. The experimental results in this segment verify the effectiveness of

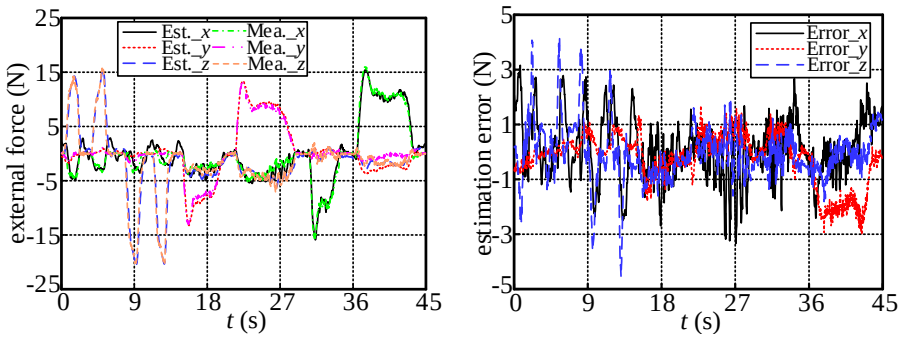

(a) External force

(b) Estimation error

Figure 7: Comparison of estimated force and measured force.

Table 2: Maximum and RMS values of force estimation errors

	Error in x	Error in y	Error in z
Maximum value (N)	3.34	3.02	4.56
RMS value (N)	1.14	0.91	1.02

the proposed end-effector force estimation approach.

The second segment is to illustrate the effectiveness of the proposed FEAE approach under the admittance control framework. Some pictures of this experiment are shown in Fig. 8.

To better demonstrate the superiority of the FEAE approach in enhancing the force exertion capability in the vertical direction, a constant payload is employed in this direction instead of human hands, as shown in Fig. 8d. The virtual joint torque limit vector is defined as $\tau_{m\,\mathrm{lim}} = [40, 40, 40, 40, 16, 16, 16]^{\mathrm{T}}$ Nm for the manipulator. The WMM configuration without FEAE is shown in Fig. 5a. The estimated external force and the resultant end-effector displacement are shown in Fig. 9, and the corresponding joint torque output is presented in Fig. 11a.

For the motion in the horizontal plane, the user could lead the WMM with a relatively small force, as shown in time 0–27.4 s. For example, at time 11 s, a

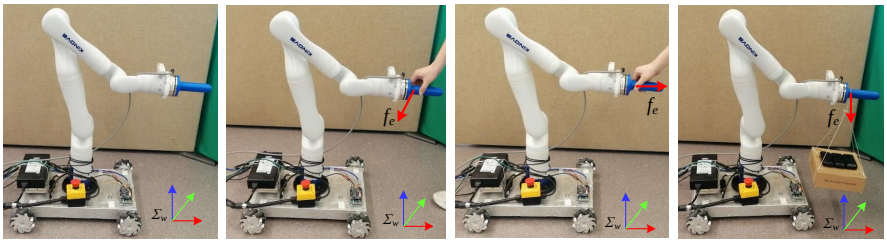

(a) (b) (c) (d)

Figure 8: Pictures of admittance control of the WMM system with FEAE. (a) shows the initial pose of the WMM, (b) shows the system's reaction when a y force exerted, (c) shows the system's response when an x force applied, and (d) shows the system's response when a z force exerted.

y force of 10.9 N could achieve a y motion speed of about 5.31 cm/s. For the motion in the vertical direction, when a payload of approximately 10 N applied during time 33.4–37.1 s, the WMM could support it with a z displacement of about 0.69 cm. However, with a payload of approximately 30 N added at time 52.5 s, the WMM could not bear it due to the saturation of joint 2 (shown in Fig. 11a), and also an unexpected x motion for the mobile base was triggered.

Then, the proposed method's performance is tested with the WMM configuration shown in Fig. 5b. The external force and the end-effector displacement are provided in Fig. 10 with the corresponding joint torque shown in Fig. 11b. It is worth mentioning that the entire system was first reconfigured with FEAE via the null-space controller, which was not shown in the figures since no external force was applied. The compliant motion in the horizontal plane can also be guaranteed in this scenario. At time 24 s, an x motion speed of about 5.57 cm/s could be generated with an external force of 14 N applied in the corresponding direction. With the proposed FEAE approach, the desired admittance behaviour can also be achieved in the vertical direction. As shown in Fig. 10, with a payload of about 31 N applied at time 37.9 s, the end-effector could generate a displacement of approximately 1.96 cm in the corresponding direction with no joint saturated.

As shown in Fig. 11, with the FEAE approach, the joint torques were also

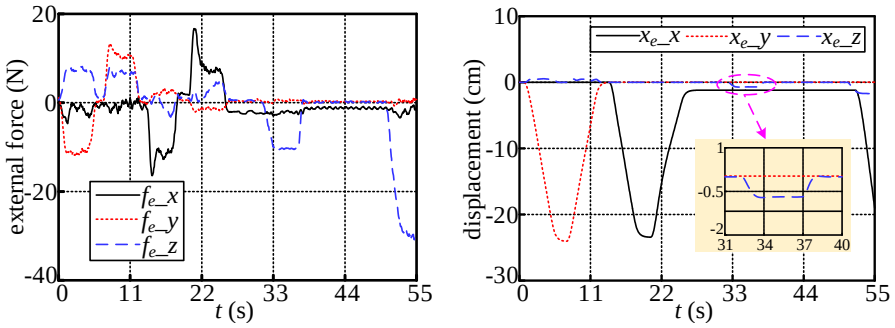

(a) External force (b) End-effector displacement

Figure 9: Estimated end-effector force and resultant displacement without FEAE.

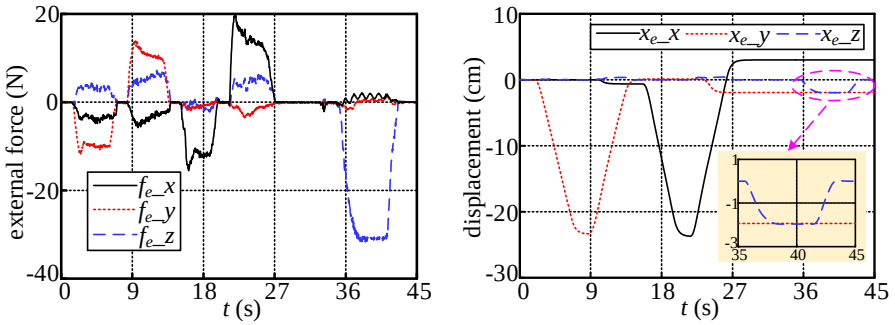

(a) External force (b) End-effector displacement

Figure 10: Estimated end-effector force and resultant displacement with FEAE.

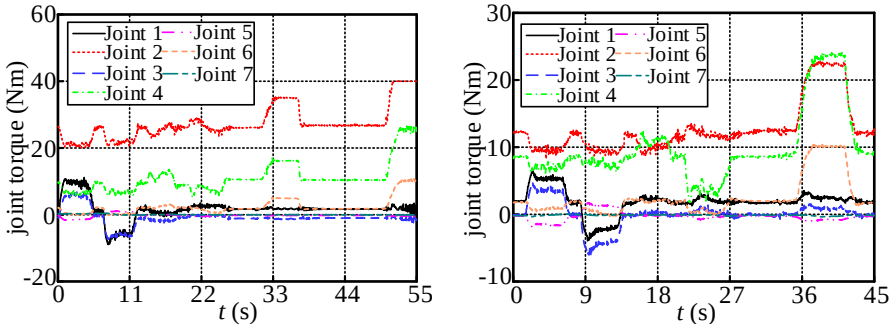

(a) Without FEAE (b) With FEAE

Figure 11: Joint torque output of the manipulator with two different configurations.

much smaller when no external disturbance exerted. For example, the torque of joint 2 was about 26 Nm (shown in Fig. 11a at time 45 s) when no FEAE was adopted, and its value decreased to about 8.5 Nm (shown in Fig. 11b at time 29 s) when FEAE was employed. Also, when a z force was applied, the manipulator could generate the same admittance behaviour using a smaller joint torque output with FEAE approach: take time of 35.00 s without FEAE experiment and 35.63 s with FEAE experiment for example, where the estimated x forces for both were about 10.3 N. However, the weighted joint torque $\|\tau_{mw}\|_2$ with gravity subtracted was reduced from 1.04 Nm to 0.61 Nm, which proves the effectiveness of the proposed approach in maximizing the end-effector exertion capability through enlarging the allowable Cartesian displacement in a given direction. It is worth noting that the system's behaviour in the horizontal plane was compliant, so no substantial joint torque was generated, which is also illustrated in Fig. 11.

5. Conclusions

In this paper, a novel robotic assistive system (RAS) to realize walking assistance for the elderly via admittance control of a wheeled mobile manipulator (WMM) with force exertion ability enhancement (FEAE) is proposed. The WMM system can provide the user with gravity support and be led by the user in the horizontal plane. Without using a pricey F/T sensor, the end-effector force is estimated based on a nonlinear disturbance observer, avoiding the need of joint acceleration measurement. An FEAE approach is employed with a null-space controller to improve the system's ability to generate high-quality admittance performance, usually limited by the restrained joint torque output. The effectiveness of the proposed approach has been experimentally verified with a 4-wheel mobile manipulator. During the FEAE experiment, the optimization objective was improved by 105.73%, and the increasing speed of the weighted joint torque with z displacement was declined by 25.86%. In the admittance control experiment, the accuracy of the force estimation approach

was verified using a wrist F/T sensor, and the results show that the maximum force estimation error was no more than 8% of its corresponding force measurement range. With the FEAE approach, the obtained Cartesian stiffness in the vertical direction was approximately 1582 N/m with a 5.47% stiffness error, and the stiffness in the horizontal plane was almost zero. The weighted joint torque (manipulator gravity subtracted) was reduced from 1.04 Nm to 0.61 Nm with the FEAE method implemented when a z force of 10.3 N was applied. Our future work will focus on predicting the user's gait to provide better assistance performance and stability assurance, and making the RAS more intelligent via learning from demonstration approach.

Acknowledgements

This work was supported by Canada Foundation for Innovation (CFI), the Natural Sciences and Engineering Research Council (NSERC) of Canada, the Canadian Institutes of Health Research (CIHR), the Alberta Advanced Education Ministry, the Alberta Economic Development, Trade and Tourism Ministry's grant to Centre for Autonomous Systems in Strengthening Future Communities, the National Natural Science Foundation of China (Grant No. 51822502, 91948202), the National Key Research and Development Program of China (No. SQ2019YFB130016), the Fundamental Research Funds for the Central Universities (Grant No. HIT.BRETIV201903), the "111" Project (Grant No. B07018), and the China Scholarship Council under Grant [2019]06120165.

References

[1] M. M. Martins, C. P. Santos, A. Frizera-Neto, R. Ceres, Assistive mobility devices focusing on smart walkers: Classification and review, Robotics and Autonomous Systems 60 (4) (2012) 548–562.

[2] A. F. Neto, A. Elias, C. Cifuentes, C. Rodriguez, T. Bastos, R. Carelli, Smart Walkers: Advanced Robotic Human Walking-Aid Systems, Springer International Publishing, Cham, 2015, pp. 103–131.

[3] M. Tavakoli, J. Carriere, A. Torabi, Robotics, smart wearable technologies, and autonomous intelligent systems for healthcare during the covid-19 pandemic: An analysis of the state of the art and future vision, Advanced Intelligent Systems 0 (0) (2020) 2000071.

[4] S. Itadera, E. Dean-Leon, J. Nakanishi, Y. Hasegawa, G. Cheng, Predictive optimization of assistive force in admittance control-based physical interaction for robotic gait assistance, IEEE Robotics and Automation Letters 4 (4) (2019) 3609–3616.

[5] M. Martins, C. Santos, A. Frizera, R. Ceres, A review of the functionalities of smart walkers, Medical engineering & physics 37 (10) (2015) 917–928.

[6] H. Xing, K. Xia, L. Ding, H. Gao, G. Liu, Z. Deng, Unknown geometrical constraints estimation and trajectory planning for robotic door-opening task with visual teleoperation assists, Assembly Automation 39 (3) (2019) 479–488.

[7] E. Dean-Leon, B. Pierce, F. Bergner, P. Mittendorfer, K. Ramirez-Amaro, W. Burger, G. Cheng, Tomm: Tactile omnidirectional mobile manipulator, in: 2017 IEEE International Conference on Robotics and Automation (ICRA), IEEE, 2017, pp. 2441–2447.

[8] C. Zhu, M. Oda, M. Yoshioka, T. Nishikawa, S. Shimazu, X. Luo, Admittance control based walking support and power assistance of an omnidirectional wheelchair typed robot, in: 2010 IEEE International Conference on Robotics and Biomimetics, IEEE, 2010, pp. 381–386.

[9] M. Spenko, H. Yu, S. Dubowsky, Robotic personal aids for mobility and monitoring for the elderly, IEEE Transactions on Neural Systems and Rehabilitation Engineering 14 (3) (2006) 344–351.

[10] M. F. Jiménez, M. Monllor, A. Frizera, T. Bastos, F. Roberti, R. Carelli, Admittance controller with spatial modulation for assisted locomotion us-

ing a smart walker, Journal of Intelligent & Robotic Systems 94 (3-4) (2019) 621–637.

[11] M. H. Raibert, J. J. Craig, Hybrid Position/Force Control of Manipulators, Journal of Dynamic Systems, Measurement, and Control 103 (2) (1981) 126–133.

[12] N. Hogan, Impedance control: An approach to manipulation: Parts I-III, Journal of Dynamic System, Measurement, and Control 107 (1) (1985) 1–24.

[13] C. Ott, R. Mukherjee, Y. Nakamura, Unified impedance and admittance control, in: 2010 IEEE International Conference on Robotics and Automation, IEEE, 2010, pp. 554–561.

[14] J. Carriere, J. Fong, T. Meyer, R. Sloboda, S. Husain, N. Usmani, M. Tavakoli, An admittance-controlled robotic assistant for semi-autonomous breast ultrasound scanning, in: 2019 International Symposium on Medical Robotics (ISMR), IEEE, 2019, pp. 1–7.

[15] J. Fong, M. Tavakoli, Kinesthetic teaching of a therapist's behavior to a rehabilitation robot, in: 2018 International Symposium on Medical Robotics (ISMR), IEEE, 2018, pp. 1–6.

[16] T. Osa, S. Uchida, N. Sugita, M. Mitsuishi, Hybrid rate—admittance control with force reflection for safe teleoperated surgery, IEEE/ASME Transactions on Mechatronics 20 (5) (2015) 2379–2390.

[17] S. Katsura, Y. Matsumoto, K. Ohnishi, Modeling of force sensing and validation of disturbance observer for force control, IEEE Transactions on industrial electronics 54 (1) (2007) 530–538.

[18] A. Mohammadi, M. Tavakoli, H. J. Marquez, F. Hashemzadeh, Nonlinear disturbance observer design for robotic manipulators, Control Engineering Practice 21 (3) (2013) 253–267.

[19] W.-H. Chen, J. Yang, L. Guo, S. Li, Disturbance-observer-based control and related methods—an overview, IEEE Transactions on Industrial Electronics 63 (2) (2015) 1083–1095.

[20] J. W. Jeong, P. H. Chang, K. B. Park, Sensorless and modeless estimation of external force using time delay estimation: application to impedance control, Journal of mechanical science and technology 25 (8) (2011) 2051.

[21] A. De Luca, G. Oriolo, P. R. Giordano, Kinematic modeling and redundancy resolution for nonholonomic mobile manipulators, in: Proceedings 2006 IEEE International Conference on Robotics and Automation, 2006. ICRA 2006., IEEE, 2006, pp. 1867–1873.

[22] A. De Luca, L. Ferrajoli, Exploiting robot redundancy in collision detection and reaction, in: 2008 IEEE/RSJ International Conference on Intelligent Robots and Systems, IEEE, 2008, pp. 3299–3305.

[23] S. Haddadin, A. De Luca, A. Albu-Schäffer, Robot collisions: A survey on detection, isolation, and identification, IEEE Transactions on Robotics 33 (6) (2017) 1292–1312.

[24] J. Koivumäki, J. Mattila, Stability-guaranteed force-sensorless contact force/motion control of heavy-duty hydraulic manipulators, IEEE Transactions on Robotics 31 (4) (2015) 918–935.

[25] A. Karami, H. Sadeghian, M. Keshmiri, G. Oriolo, Hierarchical tracking task control in redundant manipulators with compliance control in the null-space, Mechatronics 55 (2018) 171–179.

[26] A. Torabi, K. Zareinia, G. R. Sutherland, M. Tavakoli, Dynamic reconfiguration of redundant haptic interfaces for rendering soft and hard contacts, IEEE Transactions on Haptics 0 (0) (2020).

[27] H. Zhang, Y. Jia, N. Xi, Sensor-based redundancy resolution for a nonholonomic mobile manipulator, in: 2012 IEEE/RSJ International Conference on Intelligent Robots and Systems, IEEE, 2012, pp. 5327–5332.

[28] T. Yoshikawa, Manipulability of robotic mechanisms, The International Journal of Robotics Research 4 (2) (1985) 3–9.

[29] A. Torabi, M. Khadem, K. Zareinia, G. R. Sutherland, M. Tavakoli, Application of a redundant haptic interface in enhancing soft-tissue stiffness discrimination, IEEE Robotics and Automation Letters 4 (2) (2019) 1037–1044.

[30] B. Bayle, J.-Y. Fourquet, M. Renaud, Manipulability of wheeled mobile manipulators: Application to motion generation, The International Journal of Robotics Research 22 (7-8) (2003) 565–581.

[31] S. L. Chiu, Task compatibility of manipulator postures, The International Journal of Robotics Research 7 (5) (1988) 13–21.

[32] A. Ajoudani, N. G. Tsagarakis, A. Bicchi, Choosing poses for force and stiffness control, IEEE Transactions on Robotics 33 (6) (2017) 1483–1490.

[33] O. Chuy, Y. Hirat, Z. Wang, K. Kosuge, Approach in assisting a sit-to-stand movement using robotic walking support system, in: 2006 IEEE/RSJ International Conference on Intelligent Robots and Systems, IEEE, 2006, pp. 4343–4348.

[34] D. Chugo, T. Asawa, T. Kitamura, S. Jia, K. Takase, A rehabilitation walker with standing and walking assistance, in: 2008 IEEE/RSJ International Conference on Intelligent Robots and Systems, IEEE, 2008, pp. 260–265.

[35] W. Li, Z. Liu, H. Gao, X. Zhang, M. Tavakoli, Stable kinematic teleoperation of wheeled mobile robots with slippage using time-domain passivity control, Mechatronics 39 (2016) 196–203.

[36] A. Escande, N. Mansard, P.-B. Wieber, Hierarchical quadratic programming: Fast online humanoid-robot motion generation, The International Journal of Robotics Research 33 (7) (2014) 1006–1028.

[37] H. Xing, A. Torabi, L. Ding, H. Gao, Z. Deng, M. Tavakoli, Enhancement of force exertion capability of a mobile manipulator by kinematic reconfiguration, IEEE Robotics and Automation Letters 5 (4) (2020) 5842–5849.

[38] W. Yu, J. Rosen, X. Li, Pid admittance control for an upper limb exoskeleton, in: Proceedings of the 2011 American control conference, IEEE, 2011, pp. 1124–1129.

[39] W.-H. Chen, D. J. Ballance, P. J. Gawthrop, J. O'Reilly, A nonlinear disturbance observer for robotic manipulators, IEEE Transactions on Industrial Electronics 47 (4) (2000) 932–938.

[40] E. Akdoğan, M. E. Aktan, A. T. Koru, M. S. Arslan, M. Atlıhan, B. Kuran, Hybrid impedance control of a robot manipulator for wrist and forearm rehabilitation: Performance analysis and clinical results, Mechatronics 49 (2018) 77–91.

[41] K. Xia, H. Xing, L. Ding, H. Gao, G. Liu, Z. Deng, Virtual decomposition based modeling for multi-dof manipulator with flexible joint, IEEE Access 7 (2019) 91582–91592.

[42] F. Chen, M. Selvaggio, D. G. Caldwell, Dexterous grasping by manipulability selection for mobile manipulator with visual guidance, IEEE Transactions on Industrial Informatics 15 (2) (2018) 1202–1210.